Microporous and Mesoporous Materials 121 (2009) 194–199

Contents lists available at ScienceDirect

Microporous and Mesoporous Materials

journal homepage: www.elsevier.com/locate/micromeso

Synthesis and characterization of organic-functionalized molecular sieves Ph-SAPO-5 and Ph-SAPO-11

D. Zhou [a], X.-B. Luo [a], H.-L. Zhang [b], C. Dong [a], Q.-H. Xia [a,*], Z.-M. Liu [c], F. Deng [b]

[a] Ministry-of-Education Key Laboratory for the Synthesis and Application of Organic Functional Molecules, Hubei University, Wuhan 430062, PR China
[b] State Key Laboratory of Magnetic Resonance and Atomic and Molecular Physics, Wuhan Center for Magnetic Resonance, Chinese Academy of Sciences, Wuhan 430071, PR China
[c] Laboratory of Natural Gas Utilization and Applied Catalysis, Dalian Institute of Chemical Physics, Chinese Academy of Sciences, Dalian 116023, PR China

ARTICLE INFO

Article history:
Received 4 November 2008
Received in revised form 16 January 2009
Accepted 30 January 2009
Available online 6 February 2009

Keywords:
Organic-functionalization
Microporous molecular sieve
SAPO-5
SAPO-11

ABSTRACT

Organic-functionalized molecular sieves silicoaluminophosphates with AFI and AEL topologies have been first hydrothermally synthesized by using 1,4-bis(triethoxysilyl) benzene (BTEB) as unique silicon source. Various techniques have been performed to characterize the structures of the two molecular sieves. Powder XRD, solid-state ^{13}C CP/MAS NMR, FT-IR, UV–vis, and TGA analysis prove that there are aromatic groups in the final products, and ^{29}Si MAS NMR spectra demonstrate that two types of ^{29}Si chemical environments, i.e. organic T-type and inorganic Q-type silicon, coexist in the structures. The contents of organic groups are determined to be high up to 12 wt%.

1. Introduction

Zeolites, a kind of microporous crystalline materials with uniform pores, play an important role in the industrial technologies such as shape-selective catalysis, sorption, separation, ion-exchange, host–guest assemblies, etc. [1–5]. Traditional zeolites refer to aluminosilicates constructed from TO_4 tetrahedra (T = Si and Al). In 1980s, a class of zeolite-like molecular sieves aluminophosphate $AlPO_4$-*n* (*n* denotes a structure type) are developed, which are built up from strict alternation of AlO_4 and PO_4 tetrahedra [6,7]. Incorporation of silicon into the framework of $AlPO_4$-*n* yield silicoaluminophosphates (SAPOs), which are a kind of molecular sieves with moderate acidity, and exhibit considerable importance as catalysts towards the isomerization of *n*-alkanes [8,9].

Over the past decade, organic-functionalized porous materials have been developed rapidly due to their unique structural features, properties, and potential applications in shape-selective catalysis and separation [10–15]. Owing to high thermal/hydrothermal stability and good mechanical strength, the synthesis of organic-functionalized microporous crystalline materials are particularly attracting much attention [16–27]. According to the reports, various organic compounds have been used as organic source, such as organosilane (with bridging or terminal organic groups) and organic phosphonic acid, and the connection between organic groups and inorganic frameworks are different. The first hybrid microporous aluminophosphate was synthesized by using methylphosphonic acid as unique phosphorus source, in which CH_3- groups are directly bonded with framework P atoms [17]. In 1998, organic-functionalized zeolite with BEA topology was synthesized with phenethyltrimethoxysilane (PETMS, $C_6H_5(CH_2)_2$–Si-$(OCH_3)_3$) as organic silicon source, in which terminal $C_6H_5(CH_2)_2-$ groups were attached to framework Si atoms and hung within the pores [19]. In 2003, Tatsumi et al. reported the synthesis of ZOL (Zeolites containing Organic groups as Lattice) with MFI and LTA structures, in which lattice oxygen atoms were partially superseded by $-CH_2-$ groups [20], and the maximum carbon content was *ca.* 9 wt% [24].

Up to now, hybrid microporous molecular sieves aluminosilicates with LTA, MFI, FAU, BEA, and MWW structures and aluminophosphate with VFI structure have been successfully obtained. In this work, microporous silicoaluminophosphates SAPO-5 and SAPO-11 functionalized by bridging phenylene and terminal phenyl groups are first hydrothermally synthesized by using 1,4-bis(triethoxysilyl)benzene (BTEB) as unique silicon source.

2. Experimental section

2.1. Preparation of organic silicon source

Organic silicon source BTEB was prepared by the method reported in the literature [28]. The purity of 99% was confirmed by IR (Supplementary Fig. S1) and ^1H NMR (Supplementary Fig. S2) spectra, respectively.

* Corresponding author. Tel./fax: +86 27 50865370.
E-mail address: xia1965@yahoo.com (Q.-H. Xia).

1387-1811/$ - see front matter © 2009 Elsevier Inc. All rights reserved.
doi:10.1016/j.micromeso.2009.01.033

2.2. Synthesis of Ph-SAPO-5 and Ph-SAPO-11

2.2.1. Synthesis of Ph-SAPO-5

Two solutions, one of which was prepared by dissolving pseudoboehmite (66.7 wt% Al_2O_3) in the mixture of orthophosphoric acid (85 wt%) and deionized water, the other by dissolving BTEB in the mixture of triethylamine (TEA, *ca.* 10 drops) and deionized water under ultrasonic vibration, were mixed together under stirring, followed by addition of the rest TEA drop by drop. The final gel with molar composition of 1.0 Al_2O_3: 1.0 P_2O_5: 0.8 BTEB: 3.0 TEA: 33.0 H_2O was stirred at 333 K for 2 h, and crystallized in a 60 ml Teflon-lined stainless steel autoclave for 72–96 h at 453 K. The solid product was recovered by filtration, washed three times with deionized water and dried at 393 K overnight.

2.2.2. Synthesis of Ph-SAPO-11

A similar process as the synthesis of Ph-SAPO-5 was used for the synthesis of Ph-SAPO-11, except that di-*n*-propylamine (DPA) was used as the organic template. The molar composition of initial gel was 1.0 Al_2O_3: 1.0 P_2O_5: 0.5 BTEB: 2.0 DPA: 85.0 H_2O.

For the purpose of comparison, conventional SAPO-5 and SAPO-11 were also synthesized by using the methods reported previously [29,30].

2.3. Characterization

Powder X-ray diffraction (XRD) was performed on a Rigaku D/MAX-IIIC diffractometer with Cu K_α radiation ($\lambda = 1.5406$ Å) operating at 30 kV and 25 mA.

All NMR measurements except for the ^{29}Si MAS NMR experiments were performed with a double-resonance 4 mm probe on a Varian Infinityplus-300 spectrometer operating at a magnetic field strength of 7.0 T. The resonance frequencies at this field strength were 75.4, 78.1 and 121.3 MHz for ^{13}C, ^{27}Al, and ^{31}P, respectively. ^{1}H–^{13}C cross-polarization MAS (CP/MAS) experiments were performed with a contact time of 2 ms and a repetition time of 2 s. ^{31}P MAS NMR spectra were acquired using a single-pulse sequence with ^{1}H proton decoupling and a ^{31}P pulse width ($\pi/2$) of 2.2 μs and a repetition time of 15 s. For ^{27}Al MAS NMR experiments, the excitation pulse width was adjusted to $\pi/12$. The ^{29}Si MAS NMR experiments were performed with a double-resonance 7.5 mm probe on a Varian Infinityplus-400 spectrometer operating at a magnetic field strength of 9.4 T by using a single-pulse sequence with ^{1}H proton decoupling and a ^{29}Si pulse width ($\pi/2$) of 4.5 μs and a repetition time of 180 s. The spinning speeds were 5 kHz for ^{13}C CP/MAS and 6 kHz for ^{29}Si, ^{27}Al and ^{31}P MAS NMR experiments. The ^{13}C, ^{29}Si, ^{27}Al, and ^{31}P chemical shifts were referenced to hexamethylbenzene, tetramethylsilane, 0.1 M $Al(NO_3)_3$, and 85 wt% H_3PO_4 solutions, respectively.

The Infrared (IR) spectra were recorded on a Shimadzu IR Prestige-21 Fourier Transform Infrared Spectrophotometer. UV–vis spectra were collected on a Shimadzu UV–visible UV-2550 Spectrophotometer. Thermogravimetric analysis (TGA) was conducted on a FRC/T-1 thermal analyzer with a heating rate of 10 °C/min in air. X-ray fluorescence (XRF) analyses (Si, Al, P) were obtained on a Shimadzu XRF-1800 spectrometer. Elemental analysis was conducted on a Perkin–Elmer 2400 elemental analyzer. Nitrogen adsorption–desorption isotherms were measured by using a Quantachrome Autosorb-1 at 77.3 K after samples were outgassed at 393 K for 12 h under vacuum. The morphology of crystals was observed by using a JEOL JEM-100SX transmission electron microscopic (TEM) operating at 200 kV.

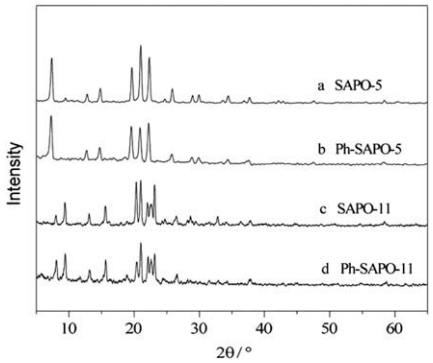

Fig. 1. XRD patterns of (a) SAPO-5, (b) Ph-SAPO-5, (c) SAPO-11, and (d) Ph-SAPO-11.

3. Results and discussion

The powder XRD patterns of Ph-SAPO-5 and Ph-SAPO-11 (Fig. 1) are in good agreement with that of conventional SAPO-5 and SAPO-11, except the difference in reflection intensity, which prove the topologies (AFI and AEL) and phase purity of the two samples.

The solid-state ^{13}C CP/MAS NMR spectra of Ph-SAPO-5 and Ph-SAPO-11 are shown in Fig. 2. In the ^{13}C CP/MAS NMR spectrum of Ph-SAPO-5 (Fig. 2a), the main resonance locating at 133.9 ppm represents phenylene carbons of Si–Ph–Si structure [31–33], and the shoulder resonance at 128.8 ppm is due to phenyl carbons of Ph–Si structure. Obviously, phenyl groups result from the cleavage of Si–C_6H_4–Si linkage. Similarly, the resonances at 133.6 ppm and

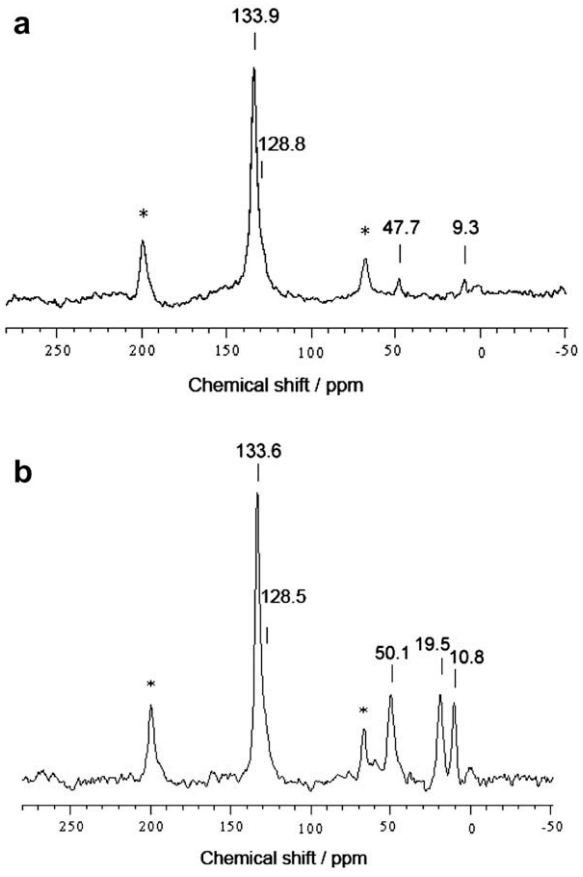

Fig. 2. ^{13}C CP MAS NMR spectra of (a) Ph-SAPO-5 and (b) Ph-SAPO-11. Asterisks (*) correspond to spinning bands.

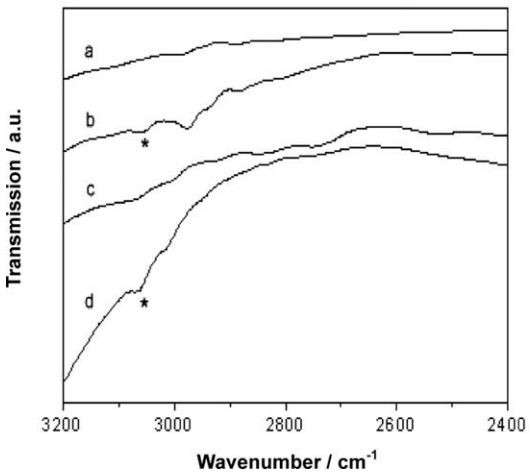

Fig. 3. FT-IR spectra of (a) SAPO-5, (b) Ph-SAPO-5, (c) SAPO-11, and (d) Ph-SAPO-11.

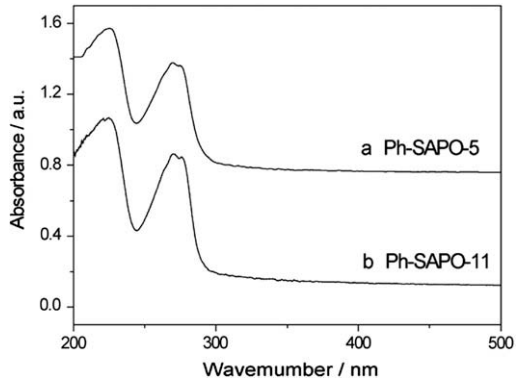

Fig. 4. UV–vis spectra of (a) Ph-SAPO-5 and (b) Ph-SAPO-11.

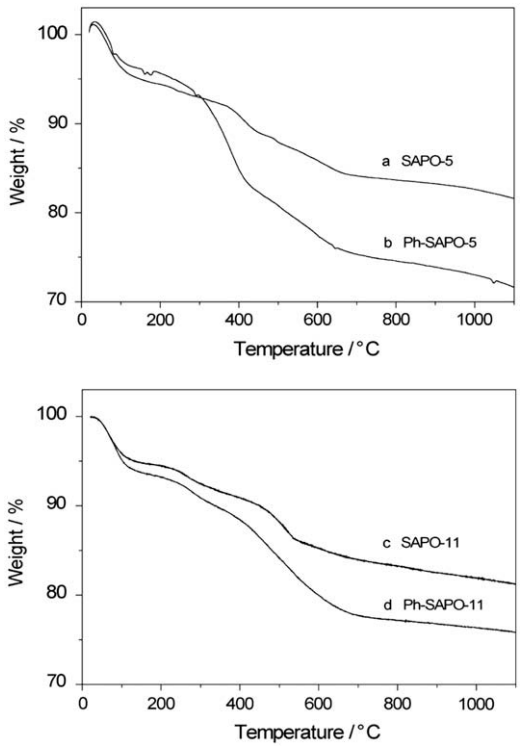

Fig. 5. TGA curves of (a) SAPO-5, (b) Ph-SAPO-5, (c) SAPO-11, and (d) Ph-SAPO-11.

128.5 ppm in Fig. 2b are assigned to carbons from phenylene and phenyl groups in Ph-SAPO-11 sample, respectively. The resonances at 47.7 and 9.3 ppm in Fig. 2a correspond to carbon atoms from CH_3– and $–CH_2–$ of TEA molecules in Ph-SAPO-5, and the resonances at 50.1, 19.5, and 10.8 ppm in Fig. 2b correspond to C^1, C^2, and C^3 atoms of DPA molecules $(C^1H_3–C^2H_2–C^3H_2)_2–NH$ in Ph-SAPO-11, respectively [33].

The existence of aromatic groups in the structures of Ph-SAPO-5 and Ph-SAPO-11 can also be supported by FT-IR, UV–vis, and TGA investigations. In the FT-IR spectra of Ph-SAPO-5 and Ph-SAPO-11 (Fig. 3), the vibrations around 3060 cm^{-1} are attributed to aromatic stretching [12], which are invisible in the spectra of conventional SAPO-5 and SAPO-11. In the UV–vis spectra of Ph-SAPO-5 and Ph-SAPO-11 (Fig. 4), the peaks centered at 227 and 275 nm are ascribable to characteristic $\pi \rightarrow \pi^*$ electron transitions of benzene ring, which shift to lower frequencies due to restricted mobility than ultraviolet adsorbances (at 203 and 254 nm) of free benzene. The TG curves of Ph-SAPO-5 and Ph-SAPO-11 (Fig. 5) show two stages of weight loss. The first weight loss below 200 °C corresponds to the loss of physically adsorbed water. The second weight loss between 200 °C and 1100 °C (*ca.* 24 wt% for Ph-SAPO-5 and 17 wt% for Ph-SAPO-11) correspond to the combustion of organic template molecules and aromatic groups, and the condensation of hydroxyl in the form of water, which are much higher than that of conventional SAPO-5 and SAPO-11 (*ca.* 12 and 13 wt%, respectively). The thermal stabilities of functionalized SAPO materials are similar to those of conventional SAPO zeolites. The XRD patterns of the two functionalized samples calcined at 1100 °C show the framework did not collapse totally, which are shown in Supplementary Fig. S3.

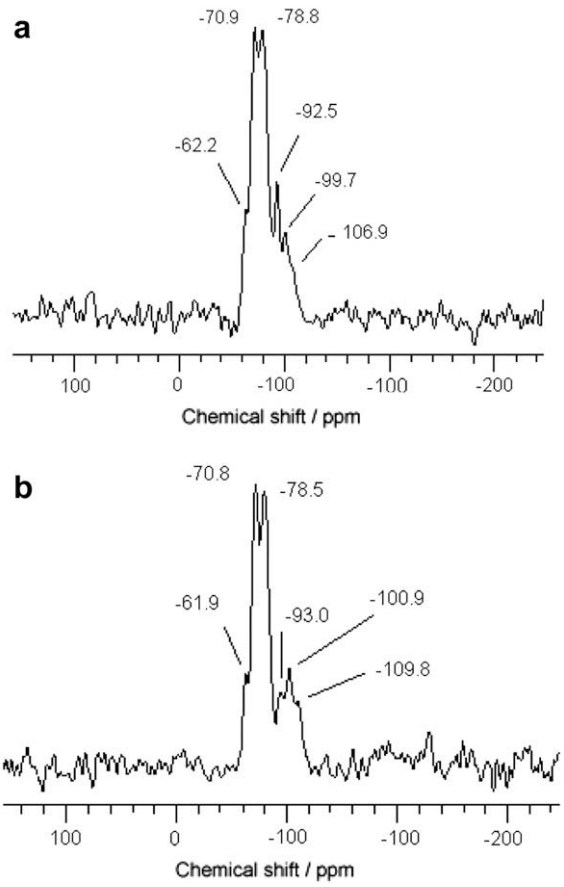

Fig. 6. ^{29}Si MAS NMR spectra of (a) Ph-SAPO-5 and (b) Ph-SAPO-11.

Table 1
The assignment of ^{29}Si Chemical Shifts of Ph-SAPO-5 and Ph-SAPO-11.

Sample	T-type Si			Q-type Si		
	T^1 $SiC(OH)_2O_b$	T^2 $SiC(OH)O_{2b}$	T^3 $SiCO_{3b}$	Q^3 $Si(OH)O_{3b}$		Q^4 SiO_{4b}
Ph-SAPO-5	−62.2	−70.9	−78.8	−92.5	−99.7	−106.9
Ph-SAPO-11	−61.9	−70.8	−78.5	−93.0	−100.9	−109.8

b: bridging oxygen, t: terminal oxygen.

Solid-state ^{29}Si MAS NMR measurements were carried out to determine the chemical environments of Si atoms in Ph-SAPO-5 and Ph-SAPO-11 (Fig. 6). Both products present various Si chemical environments. In the ^{29}Si MAS NMR spectrum of Ph-SAPO-5 (Fig. 6a), the resonances at −92.5, −99.7, and −106.9 ppm are typical of Q-type peaks of silicon, corresponding to $Q^3 \sim Q^4$ Si atoms, and the resonances at −62.2, −70.9, and −78.8 ppm originate from T-type of silicon species bonded covalently to carbon atoms, corresponding to T^1, T^2, and T^3 Si atoms, respectively [34,35]. Obviously, Si–C bonds have been preserved in the framework structure of Ph-SAPO-5. In the ^{29}Si MAS NMR spectrum of Ph-SAPO-11 (Fig. 6b), the resonances at −93.0, −100.9, and −109.8 ppm are due to Q-type of silicon atoms, and the resonances at −61.9, −70.8, and −78.5 ppm are due to T-type of silicon atoms bonded covalently to phenyl groups. For different Si coordination states, the contents of T^2 and T^3 are determined to be the highest. Detailed assignments of the ^{29}Si chemical shifts are shown in Table 1. On the basis of normalized peak areas, the intensity ratios of organic to inorganic Si (Si_T/Si_Q) for Ph-SAPO-5 and Ph-SAPO-11 are calculated to be about 3.2 and 3.0, respectively. After being degassed under vacuum at 393 K for 12 h, the calcined Ph-SAPO-5 and Ph-SAPO-11 give the multipoint BET surface areas of 303 and 168 m^2/g, respectively (see Supplementary Fig. S4), slightly smaller than those of SAPO-5 and SAPO-11.

Based on the above analyses, a possible crystallization scheme for Ph-SAPO-5 and Ph-SAPO-11 is demonstrated in Fig. 7. Firstly, Si–C_6H_4–Si linkages would be partially cleaved and produce organic (Si–C_6H_5) and inorganic Si species under hydrothermal conditions. Such a phenomenon often happens in the synthesis of organic–inorganic hybrid materials when organosilanes with bridging organic group are used as organic sources [23,24]. Secondly, thus-formed organic and inorganic Si species would co-crystallize to form Ph-SAPO-5 and Ph-SAPO-11 structures. Possible distributions of different Si coordination states in Ph-SAPO-5 and Ph-SAPO-11 have been illustrated in Fig. 7.

XRF analysis gives the molar ratio of $2SiO_2$: Al_2O_3: P_2O_5 as 1.5:1.2:1.0 for Ph-SAPO-5 sample and as 1.2:1.1:1.0 for Ph-SAPO-11 sample, different from the initial gel molar compositions (0.8:1.0:1.0) and (0.5:1.0:1.0), which imply that the Al and P source are not completely used in the crystallization. Based on elemental analysis, XRF analysis, TG results, and solid-state MAS NMR quantitative results, the contents of phenylene and phenyl groups can be approximately calculated to be *ca.* 12 wt% for Ph-SAPO-5, and 11 wt% for Ph-SAPO-11, which are the highest organic group contents for organic–inorganic hybrid microporous molecular sieves to our knowledge [24]. TEM images (Fig. 8) illustrate that the two materials are constituted of irregular crystal particles. For Ph-SAPO-5, the average crystal size was in the range of 0.2–1.2 μm, while that of Ph-SAPO-11 was larger up to 1.5–7.2 μm.

Solid-state ^{27}Al and ^{31}P MAS NMR were carried out to determine the chemical environments of Al and P in Ph-SAPO-5 and

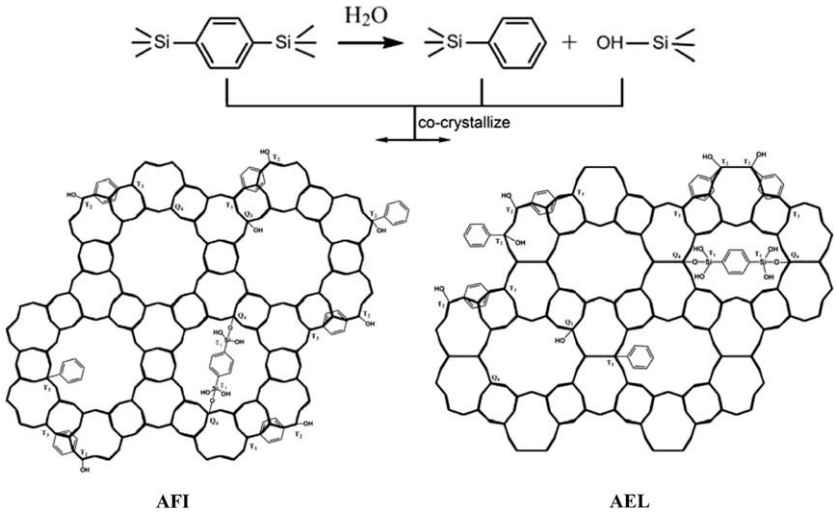

Fig. 7. Possible crystallization scheme and the distribution of different Si coordination states in Ph-SAPO-5 (AFI) and Ph-SAPO-11 (AEL).

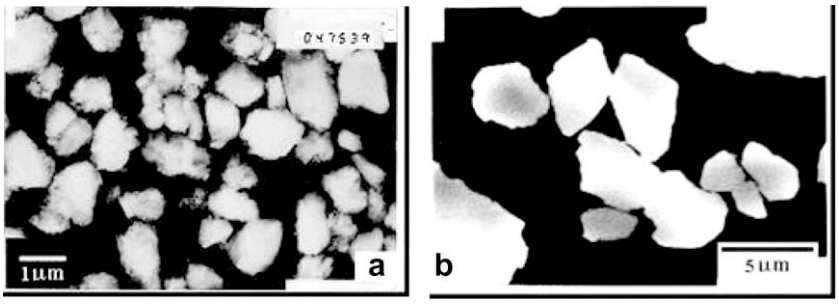

Fig. 8. TEM images of (a) Ph-SAPO-5 and (b) Ph-SAPO-11.

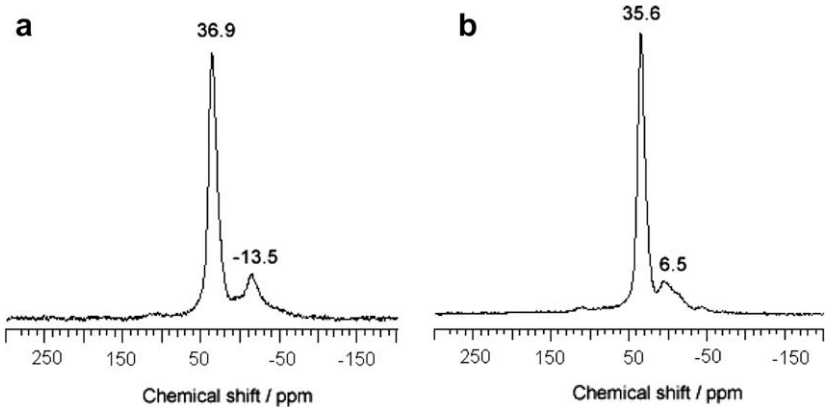

Fig. 9. ^{27}Al MAS NMR spectra of (a) Ph-SAPO-5 and (b) Ph-SAPO-11.

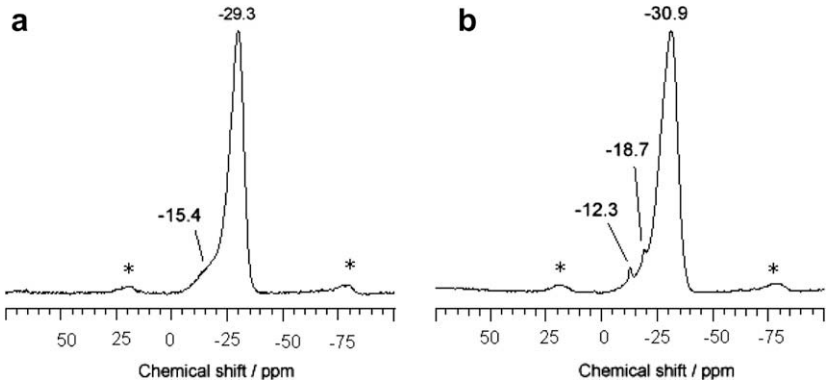

Fig. 10. ^{31}P MAS NMR spectra of (a) Ph-SAPO-5 and (b) Ph-SAPO-11. Asterisks (∗) correspond to spinning bands.

Ph-SAPO-11. In the ^{27}Al MAS NMR spectrum of Ph-SAPO-5 (Fig. 9a), the resonance at 36.9 ppm is characteristic of chemical shift for four-coordinated Al, and the resonance at −13.5 ppm is due to six-coordinated Al. In the ^{27}Al MAS NMR spectrum of Ph-SAPO-11 (Fig. 9b), the resonances at 35.6 ppm is assigned to four-coordinated Al, and the resonance at 6.5 ppm is due to the unreacted Al source [36,37]. In the ^{31}P MAS NMR spectra of Ph-SAPO-5 and Ph-SAPO-11 (Fig. 10), the strong resonances centered at −29.3 ppm and −30.9 ppm correspond to PO_{4b} (with b representing bridging oxygen). The weak resonances at −18.7, −15.4, and −12.3 ppm are due to the existence of a tiny quantity of impurities, which are invisible in XRD measurements [36,37].

4. Conclusions

Organic-functionalized molecular sieves Ph-SAPO-5 and Ph-SAPO-11 containing phenylene and phenyl groups have been first hydrothermally synthesized by using 1,4-bis(triethoxysilyl)benzene (BTEB) as unique silicon source. Various Si coordination states in the final structures come from the co-crystallization of organic Si (BTEB and Si–C_6H_5) and inorganic Si produced by the cleavage of Si–C_6H_4–Si linkage. Possible crystallization scheme and the distribution of different Si coordination states are also demonstrated. This synthesis method has been proven to be very effective for the crystallization of organic-functionalized molecular sieves with high organic group content.

Acknowledgment

The authors thank the financial supports by National Natural Science Foundation of China (No. 20673035), by the 2007 excellent mid-youth innovative team project of Hubei Provincial Education Department (no. T200701), and by Dalian Institute of Chemical Physics of Chinese Academy of Sciences.

Appendix A. Supplementary material

Supplementary data associated with this article can be found, in the online version, at doi:10.1016/j.micromeso.2009.01.033.

References

[1] D.W. Breck, Zeolite Molecular Sieves: Structure, Chemistry, and Use, Wiley, New York, 1973.
[2] A. Dyer, An Introduction to Zeolite Molecular Sieves, John Wiley and Sons, New York, 1988.
[3] N. Jappar, Q.H. Xia, T. Tatsumi, J. Catal. 180 (1998) 132.
[4] Q.H. Xia, S.C. Shen, J. Song, S. Kawi, K. Hidajat, J. Catal. 219 (2003) 74.
[5] B.L. Su, V. Norberg, Langmuir 14 (1998) 2352.
[6] S.T. Wilson, B.M.C. Lok, A. Messina, T.R. Cannan, E.M. Flanigen, J. Am. Chem. Soc. 104 (1982) 1146.
[7] J.H. Yu, R.R. Xu, Chem. Soc. Rev. 35 (2006) 593.
[8] H.O. Pastore, S. Coluccia, L. Marchese, Annu. Rev. Mater. Res. 35 (2005) 351.
[9] G.Y. Liu, P. Tian, J.Z. Li, D.Z. Zhang, F. Zhou, Z.M. Liu, Micropor. Mesopor. Mat. 111 (2008) 143.
[10] C. Sanchez, F. Ribot, New J. Chem. 18 (1994) 1007.
[11] U. Schubert, N. Husing, A. Lorenz, Chem. Mater. 7 (1995) 2010.
[12] W.F. Yan, E.W. Hagaman, S. Dai, Chem. Mater. 16 (2004) 5182.
[13] B. Hatton, K. Landskron, W. Whitnall, D. Perovic, G.A. Ozin, Acc. Chem. Res. 38 (2005) 305.
[14] W. Whitnall, T. Asefa, G.A. Ozin, Adv. Funct. Mater. 15 (2005) 1696.
[15] O. Olkhovyk, M. Jaroniec, J. Am. Chem. Soc. 127 (2005) 60.
[16] A.P. Wight, M.E. Davis, Chem. Rev. 102 (2002) 3589.
[17] K. Maeda, Y. Kiyozumi, F. Mizukami, Angew. Chem. Int. Ed. Engl. 33 (1994) 2335.
[18] A. Cauvel, D. Brunel, F. Di Renzoi, P. Moreau, F. Fajula, Stud. Surf. Sci. Catal. 94 (1995) 286.
[19] C.W. Jones, K. Tsuji, M.E. Davis, Nature 393 (1998) 52.

[20] K. Tsuji, C.W. Jones, M.E. Davis, Micropor. Mesopor. Mat. 29 (1999) 339.
[21] C.W. Jones, K. Tsuji, M.E. Davis, Micropor. Mesopor. Mat. 33 (1999) 223.
[22] C.W. Jones, M. Tsapatsis, T. Okubo, M.E. Davis, Micropor. Mesopor. Mat. 42 (2001) 21.
[23] K. Yamamoto, Y. Sakata, Y. Nohara, Y. Takahashi, T. Tatsumi, Science 300 (2003) 470.
[24] U. Díaz, J.A. Vidal-Moya, A. Corma, Micropor. Mesopor. Mat. 93 (2006) 180.
[25] K. Yamamoto, Y. Nohara, Y. Domon, Y. Takahashi, Y. Sakata, J. Plévert, T. Tatsumi, Chem. Mater. 17 (2005) 3913.
[26] B.L. Su, M. Roussel, K. Vause, X.Y. Yang, F. Gilles, L. Shi, E. Leonova, M. Edén, X. Zou, Micropor. Mesopor. Mat. 105 (2007) 49.
[27] K. Yamamoto, T. Tatsumi, Chem. Mater. 20 (2008) 972.
[28] K.J. Shea, D.A. loy, O. Websterl, J. Am. Chem. Soc. 114 (1992) 6700.
[29] B.M. Lok, C.A. Messina, R.I. Patton, R.T. Gajek, T.R. Cannan, E.M. Flaningen, U.S. Patent 4 440 871 (1984).
[30] P. Mériaudeau, V.A. Tuan, V.T. Nghiem, S.Y. Lai, L.N. Hung, C. Naccache, J. Catal. 169 (1997) 55.
[31] Y. Goto, S. Inagaki, Micropor. Mesopor. Mat. 89 (2006) 103.
[32] C.M. Li, J. Yang, X. Shi, J. Liu, Q.H. Yang, Micropor. Mesopor. Mat. 98 (2007) 220.
[33] B. Rác, P. Hegyes, P. Forgo, Á. Molnár, Appl. Catal. A: Gen. 299 (2006) 193.
[34] Q.H. Yang, M.P. Kapoor, S. Inagaki, N. Shirokura, J.N. Kondo, K. Domen, J. Mole. Catal. A: Chem. 230 (2005) 85.
[35] J. Morell, M. Güngerich, G. Wolter, J. Jiao, M. Hunger, P.J. Klar, M. Fröba, J. Mater. Chem. 16 (2006) 2809.
[36] (a) D. Zhou, J. Xu, J.H. Yu, L. Chen, F. Deng, R.R. Xu, J. Phys. Chem. B 110 (2006) 2131;
(b) Y.N. Huang, B.A. Demko, C.W. Kirby, Chem. Mater. 15 (2003) 2437;
(c) Y.N. Huang, R. Richer, C.W. Kirby, J. Phys. Chem. B 107 (2003) 1326.
[37] D. Zhou, L. Chen, J.H. Yu, Y. Li, W.F. Yan, F. Deng, R.R. Xu, Inorg. Chem. 44 (2005) 4391.